Intrinsic channel closing in strong-field single ionization of H_2

Stefan Pieper[1] and Manfred Lein[2]

[1]*Max-Planck-Institut für Kernphysik, Saupfercheckweg 1, 69117 Heidelberg, Germany*
[2]*Institut für Physik, Universität Kassel, Heinrich-Plett-Straße 40, 34132 Kassel, Germany*

The ionization of H_2 in intense laser pulses is studied by numerical integration of the time-dependent Schrödinger equation for a single-active-electron model including the vibrational motion. The electron kinetic-energy spectra in high-order above-threshold ionization are strongly dependent on the vibrational quantum number of the created H_2^+ ion. For certain vibrational states, the electron yield in the mid-plateau region is strongly enhanced. The effect is attributed to channel closings, which were previously observed in atoms by varying the laser intensity.

Above-threshold ionization (ATI) [1, 2] of atoms or molecules by intense laser fields stands for the absorption of more photons than needed to overcome the ionization threshold. A simple analysis of classical electron trajectories shows that electrons rescattering once from the core after the initial ionization step attain large final energies up to $10U_p$ [3–5], while direct (unscattered) electrons have a maximum energy of $2U_p$. Here, U_p denotes the ponderomotive potential. A striking phenomenon arises when high-order ATI is studied with respect to its dependence on laser intensity. For the rescattering plateau between $2U_p$ and $10U_p$, it was found in experiment [6, 7] and calculations [8–14], that a slight change in laser intensity can lead to order-of-magnitude changes in yield for groups of peaks within the plateau. Explanations were found in terms of multiphoton resonances with Rydberg states [8, 9, 15] and within the framework of quantum paths [10, 11, 16]. The spectral enhancements can be related to channel closings that occur when the (ponderomotively shifted) lowest ATI peak coincides with an effective threshold [10, 11].

In the present work, we investigate the role of molecular vibration in ATI channel closings, using the example of the H_2 molecule. Due to the additional degree of freedom, an additional energy scale is involved in the dynamics. In the case of atoms, channel closings were introduced by scanning through a certain range of laser intensities. We show that for molecules, due to the coupling between electronic and nuclear motion, *intrinsic* channel closing effects can be observed by comparing the electron-spectra for different vibrational states of the created H_2^+ ion, i.e., applying only one laser intensity.

The minimum energy of a free electron in the presence of a laser field with amplitude F_0 and frequency ω is equal to the ponderomotive potential (atomic units are used unless stated otherwise) $U_p = F_0^2/4\omega^2$, which is the quiver energy of the free oscillating electron. Therefore, the laser field modifies the ionization threshold. In non-resonant n-photon ionization of an atom, the electron carries the final kinetic energy

$$E_{\text{kin}} = n\,\omega - I_p - U_p, \qquad (1)$$

with the ionization potential I_p and integer n. The minimum number s of photons needed to free a bound electron is therefore defined through $s = \text{ceil}[(I_p + U_p)/\omega]$. By scanning

through a range of laser intensities and thus varying U_p, one can let ATI peaks disappear at the beginning of the spectrum. Such a channel closing causes build-up of electron probability near the core [8] and therefore leads to significant enhancements of groups of peaks within the rescattering plateau of the ATI spectrum. Note however, that the precise intensities at which this effect occurs deviate from the estimate based on the simple formula above [10, 11].

Dealing with *molecules*, due to the coupling of electronic and vibrational motion, energy is also transferred to the nuclei of the system, leading to the occupation of vibrationally excited states. We expect that for a given vibrational state of the created H_2^+ ion, Eq. (1) is changed to

$$E_{\text{kin}} = n\,\omega - I_p - U_p - \Delta E^v, \qquad (2)$$

where $\Delta E^v = E^v - E^0$ is the difference in vibrational energy between the vibrationally excited state v in question and the vibrational ground state. Note that I_p denotes here the adiabatic, not the vertical ionization potential [27].

Our model of the H_2 molecule consists of a single active electron, interacting with two protons that are screened by a second (inactive) electron. The electronic motion is restricted to the polarization direction of the laser field. We mention that the effect of moving nuclei in ATI of 1D H_2^+ has been studied previously [17], but not in the context of channel closings. Note that the dynamics of two active electrons coupled to the vibrational motion has been treated earlier within 1D models of H_2 [18, 19], but so far it has not been achieved to calculate ATI spectra within that approach. In the present work, the molecular alignment is perpendicular, i.e., the polarization direction is perpendicular to the nuclear motion. This choice was made to eliminate the dipole coupling between the electronic ground and first excited state of the H_2^+ ion and hence allow for high vibrational excitation in the electronic ground state [20]. This leads to the Hamiltonian

$$\widehat{H}(z, R, t) = -\frac{1}{2}\left(\frac{1}{\mu_n}\frac{d^2}{dR^2} + \frac{1}{\mu_e}\frac{d^2}{dz^2}\right) + V_n(R) + V_{\text{int}}(z, R) + E(t)z, \qquad (3)$$

where the operator $E(t)z$ with $E(t) = F(t)F_0\sin(\omega t)$ describes the interaction of the electron with the electric field of

a linearly polarized laser pulse in length gauge. The function $F(t)$ defines the pulse shape and F_0 is the maximum field amplitude. The electron coordinate and inter-nuclear distance are denoted by z and R; μ_e and μ_n denote the reduced masses of the active electron and of the two nuclei, respectively. The vibrational motion in the H_2^+ ion is incorporated in the model by inserting the exact Born-Oppenheimer ground-state potential of H_2^+,

$$V_n(R) = V_{BO}^{H_2^+}(R). \tag{4}$$

This choice reflects the assumption that the second (inactive) electron stays in the ground state at all times. The active electron interacts with the H_2^+ ion via a soft-core potential

$$V_{int}(z, R) = -\frac{1}{\sqrt{z^2 + \sigma^2(R)}}. \tag{5}$$

The idea behind this model is that the core, consisting of the proton charges screened by the inactive electron, is treated as one, singly charged object. The values of $\sigma(R)$ are fitted such that the ground-state Born-Oppenheimer potential of the H_2 model Hamiltonian matches the exact H_2 Born-Oppenheimer ground-state potential $V_{BO}^{H_2}(R)$ known from the literature [21]. A similar fitting procedure has been used previously to reproduce the Born-Oppenheimer potential of H_2^+ in a 1D model [22]. Since our model does not allow excitation of the second electron, we have excluded the Coulomb explosion channel, which has been extensively studied for example in [23].

The propagation of the time-dependent wave function is based on the split-operator method, along with 2D Fourier transformations to apply the kinetic-energy-dependent operators as simple multiplications in momentum space. The two-dimensional grid (z-spacing 0.36 a.u., R-spacing 0.05 a.u.) extends in R-direction from 0.2 a.u. to 12.95 a.u., in electronic direction from -276.3 a.u. to 276.3 a.u., corresponding to 256 and 1536 grid points, respectively. In the electronic dimension, the grid is further extended up to $|z| = 2522.7$ a.u. using a splitting technique [24]: in this outer region the 2D wave function $\Psi_{out}(z, R, t)$ is expressed as a sum of products states, i.e.,

$$\Psi_{out}(z, R, t) = \sum_j \xi_j(z, t)\zeta_j(R, t), \tag{6}$$

where $\xi_j(z, t)$ and $\zeta_j(R, t)$ are so-called canonical basis states or natural orbitals [25]. They are obtained as the eigenstates of the one-particle density matrices of the two coordinates z and R, respectively, for those portions of the wave function that are transferred to the outer region. The number of expansion terms is chosen to keep at least 99.9% of the total probability. No more than four terms were needed in each expansion. Within the outer region, the interaction potential $V_{int}(z, R)$ is replaced by the R-independent potential $V_{out}(z) = V_{int}(z, R = 2)$. The coupling between z and R is thus removed in this area, and 1D propagations can be applied separately to the functions $\xi_j(z, t)$ and $\zeta_j(R, t)$, which allows for large grids. This helps to keep the entire probability on the grid in spite of the vast electron excursions in strong pulses. It also leads to high resolution of the kinetic-energy spectra. In
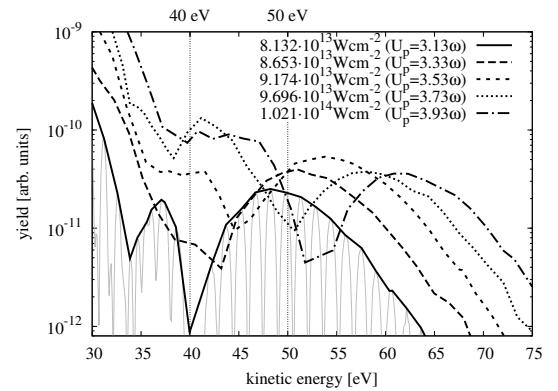

FIG. 1: Envelopes of kinetic-energy spectra of (right-going) ATI electrons leaving the H_2^+ ion in the $v = 4$ vibrationally excited state. The various laser intensities correspond to ponderomotive potentials between $U_p = 3.13\,\omega$ and $U_p = 3.93\,\omega$.

the range of $|z| = 10\ldots161$ a.u., the interaction is smoothly varied from V_{int} to V_{out}. This means that unlike [24], our calculation does not involve a discontinuity of the Hamiltonian at the boundary between inner and outer grid.

The pulse shape $F(t)$ is chosen such that the temporal pulse integral vanishes. The pulses have a plateau with constant intensity around the middle of the pulse. The leading and trailing edge of the pulses are $\sin^2$-shaped ramps. The total pulse length counts five cycles, where 1.5 cycles are used to ramp the pulse on and off, respectively. The plateau therefore extends over two cycles. After the end of the pulse, three empty cycles follow to allow for the continuum electrons to significantly escape from the Coulomb potential of the H_2^+ ion before the simulation ends. The laser wavelength is 800 nm so that we have $I_p = 10.0\,\omega$. The system is regarded as ionized for $|z| > 30$ a.u. The precise choice of this value is not important since the results shown in this work involve electrons driven at least 500 a.u. from the ion at the end of the simulation.

Projecting the ionized part Ψ_{ion} (see above) of the final wave function onto the different vibrational states χ_v of H_2^+,

$$\phi_v(z) = \int \chi_v^*(R)\, \Psi_{ion}(z, R, t_{end})\, dR, \tag{7}$$

leads to one ATI spectrum for each vibrational state considered. The spectra are calculated via Fourier transformation to $\widetilde{\phi}_v(p_z)$, followed by rescaling of the modulus square $|\widetilde{\phi}_v(p_z)|^2$ from momentum to energy. Only the right-going part of the wave function is used in this work.

According to Eq. (2), the ATI peaks within these spectra are shifted by ΔE^v. Hence, channel closings can be observed by variation of v. Since ΔE^v can easily exceed the photon energy (for the H_2^+ ion and $\lambda = 800$ nm, $\Delta E^7 \approx 1.0\,\omega$), the channel closing will always take place, no matter where exactly the first ATI peak is located. The different vibrational levels play the role of the different laser intensities in the atomic case. As soon as the vibrational energy eats up
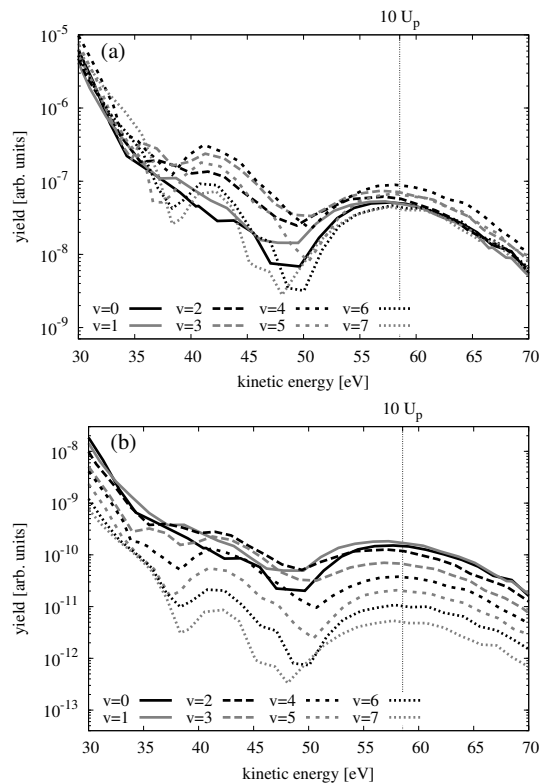
FIG. 2: Envelopes of kinetic-energy spectra of (right-going) ATI electrons produced by a laser pulse of the intensity $I = 9.696 \times 10^{13}$ W/cm^2 ($U_\mathrm{p} = 3.73\,\omega$), plotted for vibrational states of the H_2^+ ion from $v = 0, \ldots, 7$. In (a), the spectra are divided by the total yield of the corresponding vibrational state (cf. Fig. 3). In (b) the spectra show the correct weighting with respect to their yield.

enough energy, we expect that the energy spectrum for the corresponding electrons shows the characteristic channel closing features known from atoms.

In Fig. 1, kinetic-energy spectra of ATI electrons belonging to H_2^+ ions that are produced in the $v = 4$ vibrationally excited state are shown. To enhance readability, except for one example only the envelopes are plotted. Since the spectra correspond to a single vibrational state of the ion, an atom-like ATI spectrum arises for each laser intensity, and an atom-like channel closing can be identified. All spectra contain only data from the $z > 0$ part of the grid because a slight difference in peak positions between $z < 0$ and $z > 0$ would lead to blurring of the peaks. The envelope top reaches its highest value for an intensity of $I = 9.70 \times 10^{13}$ W/cm^2 ($U_\mathrm{p} = 3.73\,\omega$) at around 42 eV. Trying to estimate this intensity from in Eq. (2), the term ΔE^v is kept constant while U_p is scanned through. Using Eq. (2), we find the channel closing ($E_\mathrm{kin} = 0$) to be located at $U_\mathrm{p} = (k + 0.40)\,\omega$, with integer, non-negative k, where $k + 11 = n$, corresponding to a higher laser intensity of approximately $I = 1.14 \times 10^{14}$ W/cm^2 for $n = 15$ or a lower one of approximately $I = 8.82 \times 10^{13}$ W/cm^2 for $n = 14$. Note that these values refer to our model Hamiltonian using fitted potentials and ignoring small effects such as mass polarization.

If the laser intensity is kept fixed, but the spectra for several vibrational states of the created ion are plotted (see Fig. 2),
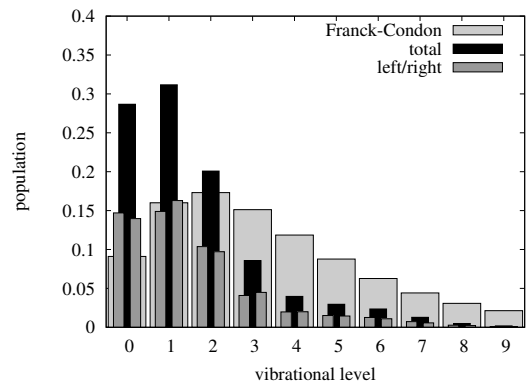

FIG. 3: Occupation of vibrational states after a laser pulse with an intensity of $I = 9.696 \times 10^{13}\,\mathrm{W/cm}^2$ ($U_\mathrm{p} = 3.73\,\omega$), split up into contributions from the left and right parts of the grid. The Franck-Condon overlap is plotted for comparison. The distribution has been normalized to total probability one .

an *intrinsic* channel closing (ICC) appears. In this case, in Eq. (2), $U_\mathrm{p} = 3.73\,\omega$ is kept fixed and ΔE^v is scanned from $v = 0$ to $v = 7$. This corresponds to values between $\Delta E^0 = 0.00\,\omega$ and $\Delta E^7 \approx 1.02\,\omega$. The amount of energy the
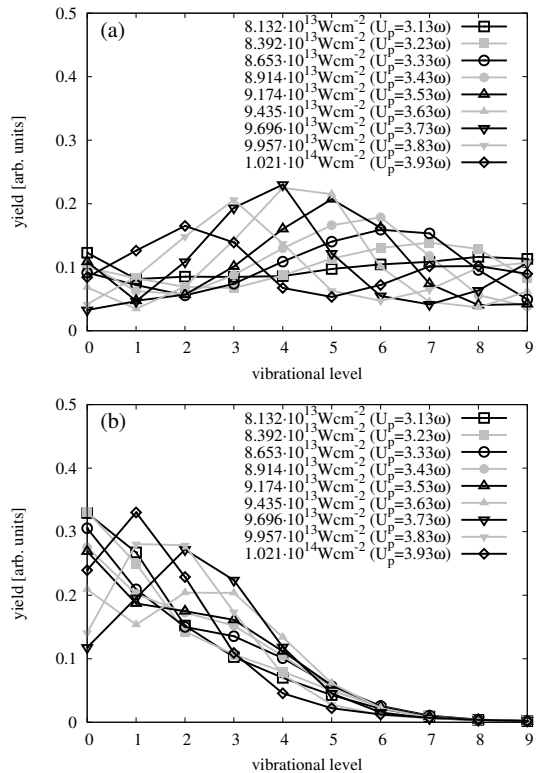

FIG. 4: Electronic yield within the energy window 40-50 eV (cf. Fig. 1), plotted versus vibrational state of the H_2^+ ion for different laser intensities. In (a), the underlying electron spectra were divided by the total yield of the corresponding vibrational state (cf. Fig. 3) as in Fig. 2(a). In (b), spectra weighted correctly with respect to their yield were taken as in Fig. 2(b).

electron loses in each case as a consequence of energy conservation shifts the spectra with respect to each other. The ICC is masked by the fact that the different vibrational states are not populated equally (see Fig. 3). Therefore, normalized spectra are plotted in Fig. 2(a), where each spectrum has been divided by the total yield of the corresponding vibrational state. The $v = 4$ spectrum shows the highest yield in the middle hump compared to all other spectra within the plot. We attribute this behavior to an ICC. The unnormalized spectra in Fig. 2(b) show the highest yield of the middle hump already at $v = 2$ due to the suppression of higher vibrational states. The application of Eq. (2) leads to $\Delta E^v = (k + 0.31)\,\omega$, where $k + 14 = n$, which corresponds to an energy difference close to the vibrational state $v = 2$ (using $n = 14$). Again, the observed position of the channel closing is shifted with respect to the one expected from Eq. (2).

It should be stressed that the energy difference between two vibrational states is larger than $0.1\,\omega$ for all vibrational states considered in this work. Hence, in contrast to the intensity scanning, the transition over a channel closing is not sampled continuously. Similar calculations for D_2 are work in progress and provide a finer graining due to the closer-lying vibrational states of the D_2^+ ion.

We show in Fig. 4, that for a suitable electron-energy window the ICC structure appears in the electron yield plotted as a function of vibrational quantum numbers. The distributions are shown using either the normalized electron yield from Fig. 2(a), see Fig. 4(a), or the unnormalized electron yield

from Fig. 2(b), see Fig. 4(b). We use the energy window between 40 and 50 eV, corresponding to the dashed vertical lines in Fig. 1. Clearly the ICC shows up in Fig. 4(a). Although the ICC feature is not as evident in the unnormalized distributions of Fig. 4(b), it is clearly visible that electrons and ions are highly correlated, since the distribution over vibrational states is, within the chosen electron-energy window, very different from the general distribution of vibrational states for all electrons. See, e.g., the curve for $U_p = 3.73\,\omega$ as compared to Fig. 3.

To summarize, we found clear signatures of spectral enhancements due to channel closings occurring in ATI of H_2 by scanning through the vibrational states of the created H_2^+ ion. The explanation of this effect seems straightforward, applying energy conservation to the photon-absorbing molecule. Similar to atoms, we find that the effect occurs at intensities/vibrational states slightly different from the simple estimate based on the unperturbed ionization potential. We conclude with a note on the experimental perspectives. The populations of H_2^+ vibrational states after strong-field ionization of H_2 have been measured in [20], but a measurement in coincidence with electrons will be difficult. On the other hand, coincidence measurements similar to recent pump-probe experiments [26] appear feasible. The goal would be to measure the electron from an ionizing pump pulse, together with fragments from probe-pulse-induced Coulomb explosion of H_2^+.

[1] P. Agostini, F. Fabre, G. Mainfray, G. Petite, and N. K. Rahman, Phys. Rev. Lett. **42**, 1127 (1979).

[2] J. H. Eberly, J. Javanainen, and K. Rzążewski, Phys. Rep. **204**, 331 (1991).

[3] G. G. Paulus, W. Nicklich, H. Xu, P. Lambropoulos, and H. Walther, Phys. Rev. Lett. **72**, 2851 (1994).

[4] G. G. Paulus, W. Becker, W. Nicklich, and H. Walther, J. Phys. B **27**, L703 (1994).

[5] G. G. Paulus, W. Becker, and H. Walther, Phys. Rev. A **52**, 4043 (1995).

[6] P. Hansch, M. A. Walker, and L. D. Van Woerkom, Phys. Rev. A **55**, R2535 (1997).

[7] M. P. Hertlein, P. H. Bucksbaum, and H. G. Muller, J. Phys. B **30**, L197 (1997).

[8] H. G. Muller and F. C. Kooiman, Phys. Rev. Lett. **81**, 1207 (1998).

[9] H. G. Muller, Phys. Rev. A **60**, 1341 (1999).

[10] G. G. Paulus, F. Grasbon, H. Walther, R. Kopold, and W. Becker, Phys. Rev. A **64**, 021401(R) (2001).

[11] R. Kopold, W. Becker, M. Kleber, and G. G. Paulus, J. Phys. B **35**, 217 (2002).

[12] S. V. Popruzhenko, P. A. Korneev, S. P. Goreslavski, and W. Becker, Phys. Rev. Lett. **89**, 23001 (2002).

[13] J. Wassaf, V. Véniard, R. Taïeb, and A. Maquet, Phys. Rev. Lett. **90**, 013003 (2003).

[14] K. Krajewska, I. I. Fabrikant, and A. F. Starace, Phys. Rev. A **74**, 053407 (2006).

[15] R. M. Potvliege and S. Vučić, Phys. Rev. A **74**, 023412 (2006).

[16] R. Kopold, W. Becker, and M. Kleber, Opt. Commun. **179**, 39 (2000).

[17] A. D. Bandrauk, S. Chelkowski, and I. Kawata, Phys. Rev. A **67**, 013407 (2003).

[18] T. Kreibich, M. Lein, V. Engel, and E. K. U. Gross, Phys. Rev. Lett. **87**, 103901 (2001).

[19] S. Saugout, C. Cornaggia, A. Suzor-Weiner, and E. Charron, Phys. Rev. Lett. **98**, 253003 (2007).

[20] X. Urbain, B. Fabre, E. M. Staicu-Casagrande, N. de Ruette, V. M. Andrianarijaona, J. Jureta, J. H. Posthumus, A. Saenz, E. Baldit, and C. Cornaggia, Phys. Rev. Lett. **92**, 163004 (2004).

[21] W. Kołos, K. Szalewicz, and H. J. Monkhorst, J. Chem. Phys. **84**, 3278 (1985).

[22] B. Feuerstein and U. Thumm, Phys. Rev. A **67**, 043405 (2003).

[23] S. Chelkowski, A. D. Bandrauk, A. Staudte, and P. B. Corkum, Phys. Rev. A **76**, 013405 (2007).

[24] R. Grobe, S. L. Haan, and J. H. Eberly, Comp. Phys. Comm. **117**, 200 (1999).

[25] P.-O. Löwdin, Phys. Rev. **97**, 1474 (1955).

[26] T. Ergler, A. Rudenko, B. Feuerstein, K. Zrost, C. D. Schröter, R. Moshammer, and J. Ullrich, Phys. Rev. Lett. **97**, 193001 (2006).

[27] The adiabatic ionization potential is the difference between the total ground state energies of H_2^+ and H_2 (including nuclear motion).